HHS Public Access

Author manuscript

World J Urol. Author manuscript; available in PMC 2021 July 01.

Published in final edited form as:

World J Urol. 2020 July ; 38(7): 1631–1641. doi:10.1007/s00345-019-02989-z.

Mechanical and functional validation of a perfused, Robot-Assisted Partial Nephrectomy simulation platform using a combination of 3D Printing and hydrogel casting.

Rachel Melnyk, MS[1], **Bahie Ezzat**[2], **Elizabeth Belfast**[1], **Patrick Saba**[1], **Shamroz Farooq**[3], **Timothy Campbell**[3], **Stephen McAleavey, PhD**[2], **Mark Buckley, PhD**[2], **Ahmed Ghazi, MD, MHPE**[1]

[1]University of Rochester Medical Center, Department of Urology, 601 Elmwood Ave., Rochester, NY 14642

[2]University of Rochester, Biomedical engineering, Hajim School of Engineering, 500 Joseph C. Wilson Blvd., Rochester, NY 14611

[3]University of Rochester Medical Center, School of Medicine and Dentistry, 601 Elmwood Ave., Box 52, Rochester, NY 14642

Abstract

Corresponding Author: Ahmed Ghazi MD, MHPE, Assistant Professor of Urology, Director of Simulation Innovation Laboratory, 400 S, White Spruce Blv., Suite B, Rochester, NY 14623, Phone (585) 402-4868, ahmed_ghazi@URMC.rochester.edu.

Author's Contribution

Protocol/project development: R Melnyk, S McAleavey, M Buckley, A Ghazi.

Data collection or management: B Ezzat, E Belfast, P Saba, S Farooq, R Melnyk, A Ghazi.

Data analysis: B Ezzat, E Belfast, P Saba, S Farooq, R Melnyk, A Ghazi.

Manuscript writing/editing: R Melnyk, A Ghazi, T Campbell.

- Rachel Melnyk: Engineer of Simulation Technologies MS, Simulation Innovation Laboratory, Department of Urology
- Elizabeth Belfast: Undergraduate Department of Biomedical Engineering, Rochester Institute of Technology. Intern at Simulation Innovation Laboratory
- Patrick Saba: Simulation Technologies researcher, Simulation Innovation Laboratory, Department of Urology
- Ahmed Ghazi: Associate Professor of Urology, Director of Simulation Innovation Laboratory, Department of Urology
- Bahie Ezzat: Undergraduate Department of Biomedical Engineering, Intern at Simulation Innovation Laboratory
- Stephen McAleavey: Associate Professor of Biomedical Engineering; Associate Professor of Electrical and Computer Engineering, Rochester Center for Biomedical Ultrasound
- Mark Buckley: Assistant Professor - Department of Biomedical Engineering (RC), Center for Visual Science A&S (RC) – Joint.
- Shamroz Farooq: Medical Student
- Timothy Campbell: Medical Student

Disclosure of potential conflicts of interest

R Melnyk: None

B Ezzat: None

E Belfast: None

P Saba: None

S Farooq : None

S McAleavey: None

M Buckley: None

Research involving Human Participants and/or Animals: This research was conducted utilizing porcine kidneys. Fresh porcine kidneys were acquired through the University of Rochester veterinary research facilities.

Informed consent: no informed consent was required for this study.

Introduction and Objectives: There is a scarcity of high-fidelity, life-like, standardized and anatomically correct polymer-based kidney models for robot-assisted partial nephrectomy (RAPN) simulation training. The purpose of this technical report is to present mechanical and functional testing data as evidence for utilizing a perfused hydrogel kidney model created utilizing 3D printed injection casts for RAPN simulation and training.

Methods: Anatomically correct tumor-laden kidney models were created from 3D-printed casts designed from a patients CT scan and injected with poly-vinyl alcohol (PVA). A variety of testing methods, quantified Young's modulus in addition to comparing the functional effects of bleeding and suturing among fresh porcine kidneys and various formulations of PVA kidneys.

Results: 7% PVA at 3 freeze-thaw cycles (7%−3FT) was found to be the formula that best replicates the mechanical properties of fresh porcine kidney tissue, where mean(+−SD) values of Young's modulus of porcine tissue vs 7%−3FT samples were calculated to be **85.97(±35) kPa vs 80.97(± 9.05) kPa, 15.7(± 1.6) kPa vs 74.56(± 10) kPa** and **87.46(± 2.97) kPa vs 83.4(± 0.7) kPa** for *unconfined compression, indentation and elastography testing* respectively. No significant difference was seen in mean suture tension during renorrhaphy necessary to achieve observable hemostasis and capsular violation during a simulated perfusion at 120 mm Hg.

Conclusions: This is the first study to utilize extensive material testing analyses to determine the mechanical and functional properties of a perfused, inanimate simulation platform for RAPN, fabricated using a combination of image segmentation, 3D printing and PVA casting.

Introduction

Human cadavers are the cornerstone resource for basic anatomic and surgical skills education, providing appropriate human anatomy with all its variations. Nonetheless, their limited availability, tissue texture dissimilarities, expense and logistical difficulties limit their use to advanced procedural training at select centers (1). Despite all these major drawbacks, human cadavers remain the most widely accepted surgical training platform due to their anatomical relevance (2). When cadavers are unavailable, live animal models are an appropriate second choice for advanced skills training due to their organoleptic properties, lower cost, occasional anatomical resemblance to certain procedures and their bleeding capability. However, ethical concerns, maintenance and disposal costs also restrict their widespread use for procedural simulation (3). Various comparisons between human cadavers and live animals were both rated with a high degree of trainee satisfaction and necessity for surgical training (4,5). Human cadavers received superior anatomic relevance compared with the porcine models, making it a better option for training in procedures, whereas the bleeding during live porcine model simulation made it a more suitable training model for vascular repair (6). As such, surgical simulation is struggling to identify the ideal training platform that combines the relevant anatomy found in cadavers and live tissue properties including bleeding found in living animal models (7).

Our efforts in combining image segmentation, three-dimensional (3D) printing and hydrogel casting have provided a platform for fabricating realistic, perfused kidney phantoms with accurate anatomical/pathological features using hydrogels that can match the mechanical properties of living tissue and have the ability to reproduce intraoperative bleeding. We have

previously demonstrated this platforms ability to replicate these essential characteristics within a robot assisted partial nephrectomy (RAPN) model (8,9). The phantoms are fabricated from Polyvinyl Alcohol (PVA), a biocompatible hydrogel that can be constituted into a viscous gel by mixing commercially available PVA powder with water. A wide array of mechanical properties mimicking human tissue can be recreated from PVA by altering the density of molecular bonds achieved by varying PVA concentration and number of freeze/thaw (F/T) cycles (10). However, liquid PVA cannot be constituted into printing material and since none of the available printing filaments can reproduce human tissue properties, we developed an injection casting technique using 3D printed casts to form PVA into the intended geometry of each kidney component. The objective of this work is to determine the PVA formula that best approximates similar tissue properties of living kidney tissue components, especially the kidney cortex, using a series of mechanical tests. Custom tests were also designed to compare the functional effects of bleeding and suturing in both living and PVA kidneys.

2 Methods

A. Model fabrication

The simulated kidney phantom is based on modifications from a C.T. scan of a patient with a 4.2 cm, partially exophytic tumor and a R.E.N.A.L nephrometry score of 7x. DICOM files were imported into Mimics 21.0 (Mimics, Materialise, Belgium) and segmentation was completed for each component of the patient's kidney including; parenchyma, tumor, inferior vena cava and renal vein, abdominal aorta and renal artery, and urinary drainage system (figure 1a). Each component was then converted to a 3D mesh and imported into 3-matic 13.0 (Mimics, Materialise, Belgium) to form a computer aided design (CAD) model of the patient's anatomy (figure 1b). To fabricate the kidney model, injection casts (tumor, kidney hilum, and parenchyma) are designed from the CAD of each component by applying a Boolean (digital) subtraction to each component of a 3D model. Injection casts are then printed in hard plastic (PLA) on a Fusion3 F400-S 3D printer (Fusion3 Design; Greensboro, NC) (figure 1c). To permit the recreation of bleeding and urine leakage during the surgical simulation, hollow structures within the kidney (artery, vein, and urinary drainage system) are directly printed from a dissolvable PVA filament and coated with a PVA formula. The inner printed part is then dissolved in water resulting in hollow arterial, venous and urinary structures. The tumor, hollow vasculature, and collecting system are registered into the final kidney cast and PVA is injected, retaining the cavity geometry representative of the patient's kidney encompassing the registered vasculature (figure 1d). To replicate the entire procedure, the kidney phantom is layered in an anatomical configuration within a body cast containing posterior abdominal musculature, perinephric fat, and relevant organs (liver, colon etc) fabricated from PVA (figure 1e). One final FT cycle leads to cohesion of all the structures to replicate the connective tissue connections between intra-abdominal organs. A daVinci robot is then docked to the final body cast for the surgeon to complete the full procedural RAPN simulation (figure 1f).

B. Mechanical testing

The mechanical response of a linear, isotropic and elastic material is described by the Young's modulus (E), a parameter related to ability of a material to resist deformation, and is considered the most important variable in determining a realistic material reaction. Using a variety of testing methods, Young's modulus was quantified for different PVA formulas and compared to fresh living kidney components. Fresh porcine kidneys were used as a surrogate based on previous work demonstrating that porcine kidneys matched the material properties of human kidneys sufficiently (11,12).

I. Kidney cortex testing—Three tests were completed. (i) Unconfined uniaxial compression test involves exerting a compressive force on a sample between two smooth platens and investigating the stress-strain behavior of the material to calculate Young's modulus. (ii) Indentation testing is a nondestructive method where an indentor is pressed into the sample and the resulting forces are measured. Using an inverse finite element analysis model (IFEA), the Poisson's ratio can be determined and used to calculate E using the Hertzian contact relationship [Equation 1] (13). (iii) Elastography involves the use of ultrasound methods to measure the speed of shear waves through a sample. The speed of propagation is related to the median shear modulus by [Equation 2] which can be used to calculate E using [Equation 3]. Twelve PVA conditions in combinations of 7, 8, 9, and 10% PVA each completing either 1, 2 or 3FTs were prepared and directly compared to porcine cortex samples.

$$E = \frac{3F\left(1-\nu^2\right)}{4R^{\frac{1}{2}}d^{\frac{3}{2}}} \quad \text{Equation 1:}$$

where: E = Young's Modulus, F = force, ν = Poisson's ratio, R = radius of the indentor, d = displacement

$$G = 2\rho V_s \quad \text{Equation 2:}$$

where: G = shear modulus, ρ = density (estimated as 1000 kg/m^3), V_s= Shear wave speed

$$E = 2G(1+\upsilon) \quad \text{Equation 3:}$$

where: E = Young's Modulus, G = shear modulus, ν = Poisson's ratio

i) Unconfined Uniaxial compression test: Porcine kidneys were obtained within 24 hrs after slaughter and stored at 4 °C. Several complete horizontal slices were made through the entire kidney and cortex tissue was isolated in an approximately cubic shape. After discarding samples that contained medullary tissue or which dimensions were skewed, 32 samples were obtained and soaked in Phosphate Buffered Solution prior to testing. 10 samples of each PVA condition were cut into cubic samples measuring 20x20x10 mm (LxWxH). Using an Instron 5960 Series Universal Testing Instrument (Instron; Norwood MA), samples were placed between smooth compression plattens and dimensions were input

into the system's software suite, Bluehill Universal (Instron; Norwood MA). Samples were uniaxially compressed up to 30% strain at a rate of 10 mm/min. Young's modulus was calculated for this range and directly exported from Bluehill Universal (figure 2).

ii) Indentation test: The assumptions that satify the Hertzian relationship [Equation 1] assume an infinite sample size. Therefore, samples for porcine cortex were kept as large as possible, forming 27 rectangular samples. For each of the 12 PVA conditions, a singular large block was prepared and tested using the Instron 5960 at 10 different points across the surface. A custom spherical indenter (r=.635 mm) was prepared to allow contact a small part of the surface. Samples were uniaxially compressed up to 3 mm at a rate of 10 mm/min (figure 3a). The average maximum force obtained at a displacement of 3 mm was exported. An inverse FEA model was created in FEBio (a software package that offers modeling scenarios) to simulate the indentation test using the average sample geometry and following the same test parameters (figure 3b) (13). The result is the Poisson's ratio that was used to establish E [Equation 1].

iii) Elastography: To confirm the results of the previous tests, E was also calculated using an ultrasound elastography method. Elastography measures the speed of sound waves through a material to establish the elasticity of the material. A custom-built ultrasound utilizing the virtual touch quantification method on the Siemens Acuson 3000 scanner (Siemens-Acuson, Mountain View, CA, USA) allowed for the measurement of shear wave speed. Kidneys from each of the 12 PVA kidney conditions previously mentioned along with porcine kidneys were placed under the probe (figure 4a). Following localization and selection of an area on the image only containing the cortex (figure 4b), the shear wave speed (V_s) was directly calculated by the scanner to establish shear modulus [Equation 2], which along with the Poisson's ratio of the sample was used to calculate E [Equation 3].

II. Functional Testing—Functionally, the model is designed to recreate the effects of bleeding and suturing. Customized testing methods were established to study the flow of blood through both porcine and PVA kidneys with the aim to analyze their responses to the two types of suturing techniques used for closure of the parenchymal defect during a RAPN. These tests measured the tension applied to the first layer of running sutures required to achieve hemostasis and the tension applied to the second layer of parenchymal sutures for approximation of the parenchymal edges before tearing occurs in both an ex vivo porcine and the PVA kidney models.

i) Hemostatic closure: Fourteen porcine kidneys were obtained with premade incisions cut through the entirety of the cortex, averaging 10.5 cm in length and 12.4 mm in depth. Their renal vessels were isolated using renal transplantation techniques, with ligation of the vein and catheterization of the artery. For comparison, five PVA models for each of the best PVA conditions matching the PVA cortex: 7%−3FTs, 9%−3FTs, 10%−2FTs (PVA% and # of FTs) were created with a similar corresponding incision. An IV bag containing 18% glycerin solution with an equivalent viscosity to blood [18] was suspended at 1.63 meters to simulate blood flow at approximately 120 mmHg and a flow sensor (FT-120; Gem's, Plainville, CT) was placed in line with the IV infusion tubing (14). A 2–0 Vicryl suture on

an SH needle was run in a hemostatic manner by a urologist along the base of the entire incision and the kidney then secured in 3D printed custom rig in the setting described above (figure 5). Measurement of initial flow was collected at the beginning of the test prior to any tension being applied. The free end of the continuous suture was then placed in the grips of the Instron 5960 and tension was applied at a rate of 10 mm/s. Flow was measured after the force on the suture reached 5 N, and again once it reached 10 N. A reduction in fluid flow would signify hemostasis during a simulated perfusion at 120 mmHg based on previous work by Endres et al. (15).

ii) Renorrhaphy Sutures for parenchymal approximation: A uniaxial suture tension test was performed in accordance with a published preclinical model of sliding-clip renorrhaphy [15]. Six porcine and six kidneys of each of the best matching PVA types were prepared with a 10.5 cm long and 12.4 mm deep longitudinal incision made along the lateral kidney surface. Three, 6 inch, 0-Vicryl, CT-1 sutures with Hem-o-lok (Teleflex Medical, Research Triangle Park, NC) clips were then placed deep and equally across the incision using the sliding-clip technique (16). The kidney was placed in a specifically designed 3D printed support tray with vertical slits to allow passage of the sutures (figure 6a). Steady tension was placed on the sutures at a rate of 10 mm/s using the Instron 5960. The force needed to achieve closure of the defect, (visual coaptation of the renal capsule) (figure 6b) was recorded and continued up to the maximum force necessary to rip the clip through the parenchymal edge of each PVA and fresh porcine kidney (figure 6c).

Results

I. Mechanical Testing (Table 1)

Mean and SD values of modulus for porcine kidney cortex samples were calculated at **85.97(±35) kPa** for unconfined compression, **15.7(±1.6) kPa** for spherical indentation and **87.46(±2.97) kPa** for elastography. Shear velocity was calculated at **5.53(± 1.02) m/s** during elastography of the renal cortex. The three PVA conditions that most closely approximate modulus of porcine kidney samples were 7%−3FTs, 9%−2FTs and 10%−2FTs and calculated values at **80.97(±9.05) kPa, 91.2(±16.9) kPa** and **101.1(± 9) kPa** respectively for *unconfined compression testing*, **74.56(±10) kPa**, **91.91(±9.62) kPa** and **99.67(±9.88) kPa** respectively for *spherical indentation* and **83.4(±0.7) kPa, 91.6(±0.7) kPa** and **106.4(±0.4) kPa** respectively for *elastography*. Mean and SD values of shear wave speed calculated during elastography was **5.4(±0.49) m/s**, **5.66(± 0.5) m/s** and **6.12(± 0.36) m/s** respectively.

II. Functional Testing

During the hemostatic closure testing of the 14 fresh porcine kidneys the average initial flow rate without tension on the hemostatic sutures was **120.9 mL/min**. After applying a 5 N and 10 N tension to the continuous sutures there was a 55.0% (**54.5 mL/min**) and 65.9% (**41.2 mL/min**) reduction in flow rate during simulated perfusion at 120 mm Hg. Similar testing in 7%−3FTs, 9%−2FTs and 10%−2FTs at 5 to 10N demonstrated a 57.4% to 70.1%, 22.9% to 50.8% and 25.8% to 52.5% reduction in flow rate respectively (Table 2). During the renorrhaphy suture testing for porcine kidneys, the mean suture tension achieved during renorrhaphy necessary to approximate the parenchymal edges was **8.41N (±1.38N)** and

maximum suture tension at which the hem-o-lok clips tear through the parenchyma was **19.29N (±8.78N)**. 7%−3FTs was the PVA condition that most closely approximated suture tension of porcine kidneys during renorrhaphy with tension for parenchymal approximation and hem-o-lok clip tear through measuring **9.29N (±3.07N) and 22.36 N (±9.8N)** respectively (Table 3). 9%−2FTs and 10%−2FTs demonstrated a maximum suture tension at which the sutures tear through the parenchyma was **15.76N (±6.78N)**, and **25.59 N (±9.8)** respectively.

Discussion

Simulation-based medical education is rapidly advancing with tools such as 3D printers to assist with the development of anatomically correct polymer-based models that can provide more advanced haptic simulation for the rehearsal of highly complex procedural skills (17). Specialized fields such as robot-assisted surgery benefit from such simulation opportunities that extend beyond basic robotic skills into advanced procedure specific training, especially for the practice of technically demanding procedures as RAPN with a reported learning curve of up to 150 cases (18). 3D printing has been utilized in renal cancer cases by urologists where patient's medical images were segmented to create 3D printed physical kidney replicas depicting detailed soft tissue, vascular anatomy and complex tumors (19–22). While the current practice replicates human anatomy for the sole purpose of surgical planning, it is insufficient to achieve surgical tissue properties. Therefore, rather than directly printing a physical kidney we converted patients' imaging to 3D printed negative casts into which a hydrogel (PVA) is injected. To determine the PVA formula that mimics the mechanical properties of kidney tissues we conducted a series of mechanical tests comparing several PVA formulations to fresh porcine kidney tissue. The three types of testing used to identify the tissue strain of the kidney cortex (compression, indentation and elastography) yielded consistent results for each condition of PVA, with each method obtaining a solution within two standard deviations of the other methods (figure 7). Our testing was limited to low strains (up to 30%), as these forces represent the strain applied on tissues during surgery prior to tissue damage as reported by Farshad et al (23). Additionally, the general behavior of samples under compression is characterized by a non-linear curve that steepens sharply after 30% strain thus complicating analysis at higher strains.

Our results demonstrated that the Young's modulus of 7%−3FTs, 9%−2 FTs and 10%−2FTs fell between the mean ± .5 SD of the E of porcine kidneys during unconfined compression testing (figure 7). 7%−3FTs demonstrated the most consistent comparison to fresh porcine kidneys. A minimal difference was seen in E during unconfined compression testing between porcine cortex samples vs 7%−3FTs (Δ=5N) and 9%−2FTs (Δ=−5.23N), while 10%−2FTs demonstrated a greater difference in E from porcine cortex (Δ=−15.13N). True to the nature of PVA, with increased concentration and FT cycles, a higher E results due to increased stiffness. Similarly, a minimal difference was seen in Young's modulus during elastography testing between porcine cortex samples vs 7%−3FTs (Δ=4.06N) and 9%−2FTs (Δ=−4.14), while 10%−2FTs demonstrated a greater difference from porcine cortex (Δ= −13.46N). Indentation testing of porcine kidneys failed to match the compression and elastography results. This may be due to the fact that the assumptions satisfying the Hertzian relationship [Equation 1] used to calculate E assumes an infinite sample size. Despite an

attempt to keep the tested procine cortex samples as large as possible, there was a clear discrepancy between results from other testing types. Nevertheless, the Possion's ratio calculated from indentation testing was essential to calculate Young's modulus during elastography, and the results of elastography for porcine fell within the range of compression testing of the PVA conditions tested. Sutured parenchymal reapproximation during RAPN has been identified as one of the more challenging steps (24,25). Thus, it was essential to recreate this challenging step in our PVA models in a realistic manner by incorporation of a functional renal hilum and parenchymal bleeding during tumor resection. We customized mechanical tests to replicate closure of the renal parenchyma after removal of the tumor. The first layer closure is a running suture applied to achieve hemostasis and address violations of the vascular system at the tumor resection bed. For the second layer, the sliding clip renorrhaphy suture is the most utilized technique and approximates the parenchymal edges of the defect, promoting revascularization and healing (26).

Our results confirmed that 7%−3FT kidneys are also best suited to replicate the functional properties of porcine kidneys. During a simulated perfusion at 120 mmHg they demonstrated an average reduction in flow rate of 57.4% to 70.1% compared to 55.0% to 65.9% in porcine kidneys when applying sequential tension of 5 N and 10 N on the hemostatic continuous sutures at the incision bed. Similar testing in 9%−2FT and 10%−2FT kidneys demonstrated a lesser reduction in flow rate, 22.9% to 50.8% and 25.8% to 52.5% respectively. Likewise, the average force for approximation of the renal parenchyma up to the force required for clips to rip through the edge of the porcine cortex (8.41N up to 19.29N) was found to closely resemble 7%−3FTs PVA (9.29N up to 22.36 N). Despite 9% −2 FTs PVA demonstrating almost similar results to 7%−3FTs PVA during mechanical testing there was a significant difference during functional testing. This may be the result of increasing hydrogel stiffness hindering the coaptation of the simulated kidney parenchyma that elicits a closure pressure on the simulated blood vessels registered within the hydrogel. We found it essential to test these hydrogel kidney models in their ability to accurately simulate this key step as tension on the clips anchoring the renorrhaphy sutures must be applied with careful consideration to prevent possible kidney damage during RAPN (25,26). A significant difference in these forces was demonstrated when comparing 9%−2FTs and 10%−2FTs PVA formulations to 7%−3FTs and porcine kidneys, which may lead to a trainee applying an inappropriate force during training, resulting in kidney damage.

Recent work done by Qiu K et. al (27) used mechanical testing methods in order to characterize and recreate the properties of prostate tissue in a 3D printed prostate designed for preoperative planning and rehearsal. A total of three tissue samples were obtained and used for compression testing, resulting in Young's moduli ranging from 10.9 kPa to 25.7 kPa for a strain range of 0–15%. This testing was the main basis for their choice in material. Dynamic compression testing was completed in order to analyze the viscoelastic properties and nanoindentation tests were used to measure hardness. The optical reflections were also characterized as viewed endoscopically. This work is one of the first to use mechanical testing methods to increase fidelity, although limited by the small samples size of tissue samples tested. The final model described here was tested to withstand to manipulation by finger, endoscope, surgical grasper, and surgical scissors, but without data to justify its ability to justify it as a procedural simulation platform. Other studies have reported utilizing

materials proposed to approximate the shape and elasticity of a kidney model with similar mechanical strength that contribute to a growing body of evidence supporting the efficacy of 3D printed simulations. Von Rundstedt's robotic surgical rehearsals using rapidly produced, realistic silicone models entailed 10 patient-specific models, fabricated to duplicate their complex tumor anatomy (average R.E.N.A.L. nephrometry scores of 8.9 and mean maximal tumor diameter of 40.6 mm). The group compared the mean resection times and tumor volumes between the excised model, and excised tumor which were not significantly different. Kidney models were manufactured using mixtures of silicone rubber [shore hardness 10A, Die B tear strength of 17.863 N/mm (102 pounds/linear inch), tensile strength 3.2750 MPa (475 psi)] and silicone oil as a thinner. Model fabrication was performed by a 3rd party Lazarus 3D (Houston, TX, USA). The authors mention a series of preliminary studies, where different mixes of these materials were tested to formulate the mixture that most realistically simulated normal kidney and tumor tissue properties. However, no comment on how realism was defined, which tissue was used as a comparison or a publication for reference was provided (28). Maddox et al, 2017 quantified the benefit of pre-op rehearsals on patient outcomes using specific 3D kidney models. A simulation using the da Vinci platform was completed prior to RAPN. Significantly different outcomes reported in this study was a lower blood loss (186 ml vs 236mL, $p = 0.01$) when compared to case controls. The only description of the seven models fabricated were that they were constructed using a photopolymer resin suitable for surgical resection (agarose gel solution) to create a spongy texture with color variation to delineate the renal parenchyma, tumor, vascular structures, components of the collecting system, and the proximal ureter (29).

The use of cadavers represents the only truly anatomical simulator with the highest possible fidelity available to practice entire operations. However, to combine accurate human anatomy with physiological and circulatory conditions, human cadavers have been artificially perfused with costs approximating $1000 replicating the real-life parameters of dissection with hemostasis (30). Nevertheless, theses attempts have been limited in a significant number of cadavers by impossibility to clear the vascular tree, previous vascular or cardiac surgery, and a positive viral profile (31). Our perfused hydrogel anatomical model combines the lifelike conditions of the living tissue with real human anatomy with reasonable cost. Each model costs $43.30 in material, $60 in personnel and $82 in consumables for participant trial, thereby facilitating widespread use and individualized training. The laboratory does recognize the startup cost of a da Vinci robot and instruments, however the non-biohazardous nature of our model negates the need of a dedicated teaching robot and instruments. Furthermore, the absence of an infection risk, customizable pathology, availability, unnecessary specialized facilities, and ability to simulate complications such as bleeding (32–34) provide a significantly favorable economic valuation compared to similar procedural models.

Simulation has become widely accepted as a supplementary method of surgical training. With the rapid adoption of minimal invasive surgery many generic-skills simulators have been created for laparoscopic and robot-assisted surgery, but only a limited number of realistic procedure-specific models are available (35,36). This is the first comprehensive mechanical analyses of a polymer-based kidney model with the ability to replicate both the mechanical and functional properties of living kidney tissue, thus offering an easily

disposable, perfused and realistic platform that closely replicates key steps of a RAPN procedure.

Conclusion

This technique of combining 3D printing and hydrogel casting can be utilized to fabricate perfused kidney phantoms that depict detailed human anatomy, including a functional renal hilum. With widespread application of this technique, 3D printing can progress from use in education and pre-operative planning to realistic procedure-specific simulation of complex urological procedures.

Acknowledgments

A Ghazi: Intuitive Surgical: Research grant, Olympus America: Consultant

References

1-. Gilbody J, Prasthofer AW, Ho K, et al. The use and effectiveness of cadaveric workshops in higher surgical training: a systematic review. Ann R Coll Surg Engl 2011;93:347–352. [PubMed: 21943455]

2-. Ross HM, Simmang CL, Fleshman JW, Marcello PW. Adoption of laparoscopic colectomy: results and implications of ASCRS hands-on course participation. Surg Innov 2008;15:179–183. [PubMed: 18757376]

3-. Van Bruwaene S, Schijven MP, Napolitano D, De Win G, Miserez M. Porcine Cadaver Organ or Virtual-Reality Simulation Training for Laparoscopic Cholecystectomy: A Randomized, Controlled Trial. J Surg Educ 2015; 72(3):483–490. [PubMed: 25555673]

4-. LeBlanc F, Champagne BJ, Augestad KM, et al. A comparison of human cadaver and augmented reality simulator models for straight laparoscopic colorectal skills acquisition training. J Am Coll Surg 2010;211:250–255. [PubMed: 20670864]

5-. Ross HM, Simmang CL, Fleshman JW, Marcello PW. Adoption of laparoscopic colectomy: results and implications of ASCRS hands-on course participation. Surg Innov 2008;15:179–183. [PubMed: 18757376]

6-. Stefanidis D, Yonce TC, Green JM, Coker AP. Cadavers versus pigs: which are better for procedural training of surgery residents outside the OR? Surgery. 2013;154(1):34–7. doi: 10.1016/j.surg.2013. [PubMed: 23809483]

7-. Villegas L, Schneider BE, Callery MP, Jones D. Laparoscopic skills training. Surg Endosc 2003; 17(12):1879–88. [PubMed: 14577030]

8-. Candela B, Stone JJ, Park J, Guan W, Rashid H, Joseph J, Ghazi A. Concurrent validity of a simulated inanimate model for physical learning experience in partial nephrectomy (SIMPLE-PN). J Urol 2016;195, No. 4S, Supplement: e220.

9-. Ghazi A, Stone JJ, Candela B, Richards M and Joseph J. Simulated inanimate model for physical learning experience (SIMPLE) for robotic partial nephrectomy using a 3-D printed kidney model. J Urol 2015;193, No. 4S, Supplement: e778.

10-. Li P, Jiang S, Yu Y, Yang J, Yang Z. Biomaterial characteristics and application of silicone rubber and PVA hydrogels mimicked in organ groups for prostate brachytherapy. J Mech Behav Biomed Mater 2015;49:220–34. doi: 10.1016/j.jmbbm.2015.05.012. [PubMed: 26042767]

11-. Umale S, Deck C, Bourdet N, et al. Experimental mechanical characterization of abdominal organs: liver, kidney & spleen. Journal of the mechanical behavior of biomedical materials. 2013;17:22–33. [PubMed: 23127642]

12-. Miller K Method of testing very soft biological tissues in compression. J Biomech 2005;38(1):153–8. [PubMed: 15519351]

13-. Maas SA, Ellis BJ, Ateshian GA, Weiss JA. FEBio: Finite Elements for Biomechanics. J Biomech Eng 2012;134(1):011005. [PubMed: 22482660]

14-. Boës S, Ochsner G, Amacher R, Petrou A, Meboldt M and Schmid Daners M Control of the Fluid Viscosity in a Mock Circulation. Artif Organs. 2018 42: 68–77. doi:10.1111/aor.12948. [PubMed: 28718516]

15-. Endres DM, Bossemeyer RW, Tobert CM, Baer WH, Lane BR. Investigation of Forces Involved in Closure of the Renal Remnant After Simulated Partial Nephrectomy. Urology 2014; 84(4):971–975. [PubMed: 25096334]

16-. Benway BM, Wang AJ, Cabello JM, et al. Robotic partial nephrectomy with sliding-clip renorrhaphy: technique and outcomes. Eur Urol 2009;55:592–599. [PubMed: 19144457]

17-. Bartellas M: Three-dimensional printing and medical education: a narrative review of the literature. UOJM 2016, 6:1–38. 10.18192/uojm.v6i1.1515.

18-. Yang B, Zeng Q, Yinghao S et al. A novel training model for laparoscopic partial nephrectomy using porcine kidney. J Endourol 2009; 23: 2029–33. [PubMed: 19860575]

19-. Silberstein JL, Maddox MM, Dorsey P, Feibus A, Thomas R, Lee BR (2014) Physical models of renal malignancies using stand- ard cross-sectional imaging and 3-dimensional printers: a pilot study. Urology 84(2):268–272. 10.1016/j.urology.2014.03.042. [PubMed: 24962843]

20-. Knoedler M, Feibus AH, Lange A, Maddox MM, Ledet E, Thomas R, Silberstein JL. Individualized physical 3-dimensional kidney tumor models constructed from 3-dimensional printers result in improved trainee anatomic understanding. Urology. 2015; 85(6):1257–1261. 10.1016/j.urology.2015.02.053. [PubMed: 26099870]

21-. Zhang Y, Ge HW, Li NC, Yu CF, Guo HF, Jin SH, Liu JS, Na YQ. Evaluation of three-dimensional printing for laparoscopic partial nephrectomy of renal tumors: a preliminary report. World J Urol 2016; 34(4):533–537. 10.1007/s00345-015-1530-7. [PubMed: 25841361]

22-. Shin T, Ukimura O, Gill IS. Three-dimensional printed model of prostate anatomy and targeted biopsy-proven index tumor to facilitate nerve-sparing prostatectomy. Eur Urol 2016; 69(2):377–379. 10.1016/j.eururo.2015.09.024. [PubMed: 26431913]

23-. Farshad M, Barbezat M, Flueler P, Schmidlin F et al. Material characterization of the pig kidney in relation with the biomechanical analysis of renal trauma. J Biomech 1999;32:417–425. [PubMed: 10213032]

24-. Canales BK, Lynch AC, Fernandes E, et al. Novel technique of knotless hemostatic renal parenchymal suture repair during laparoscopic partial nephrectomy. Urology. 2007;70:358–359. [PubMed: 17826508]

25-. Patel MN, Menon M, Rogers CG. Robotic partial nephrectomy: a comparison to current techniques. Urol Oncol 2010;28:74–7. [PubMed: 20123352]

26-. Benway BM, Wang AJ, Cabello JM, et al. Robotic partial nephrectomy with sliding-clip renorrhaphy: technique and outcomes. Eur Urol 2009;55:592–599. [PubMed: 19144457]

27-. Qiu K, Zhao Z, Haghiashtiani G, et al. 3D Printed Organ Models with Physical Properties of Tissue and Integrated Sensors. Adv Mater Technol 2018;3(3):170–235.

28-. Von Rundstedt FC, Scovell JM, Agrawal S, et al. Utility of patient-specific silicone renal models for planning and rehearsal of complex tumour resections prior to robot-assisted laparoscopic partial nephrectomy. BJU Int 2017; 119(4): 598–604. [PubMed: 27862866]

29-. Maddox MM, Feibus A, Liu J, et al. 3D-printed soft-tissue physical models of renal malignancies for individualized surgical simulation: a feasibility study. J Robot Surg 2018; 12(1): 27–33. [PubMed: 28108975]

30-. Carey JN, Minneti M, Leland HA, et al. Perfused fresh cadavers: method for application to surgical simulation. Am J Surg 2015;210:179–87. [PubMed: 25890815]

31-. Faure JP, Breque C, Danion J, Delpech PO, Oriot D, Richer JP. SIM Life: a new surgical simulation device using a human perfused cadaver. Surg Radiol Anat 2017;39:211–217. [PubMed: 27315801]

32-. Udomsawaengsup S, Pattana-arun J, Tansatit T, et al. Minimally invasive surgery training in soft cadaver (MIST-SC). J Med Assoc Thai 2005;88:189–194.

33-. Giger U, Fresard I, Hafliger A, Bergmann M, Krähenbühl L. Laparoscopic training on Thiel human cadavers: a model to teach advanced laparoscopic procedures. Surg Endosc 2008;22:901–906. [PubMed: 17704868]

34-. Supe A, Dalvi A, Prabhu R, Kantharia C, Bhuiyan P. Cadaver as a model for laparoscopic training. Indian J Gastroenterol 2005;24:111–113. [PubMed: 16041103]

35-. Moglia A, Ferrari V, Morelli L, Ferrari M, Mosca F, Cuschieri A. A Systematic Review of Virtual Reality Simulators for Robot-assisted Surgery. Eur Urol 2016;69:1065–80. [PubMed: 26433570]

36-. Ahmed K, Jawad M, Abboudi M et al. Effectiveness of procedural simulation in urology: a systematic review. J Urol 2011; 186: 26–34. [PubMed: 21571338]

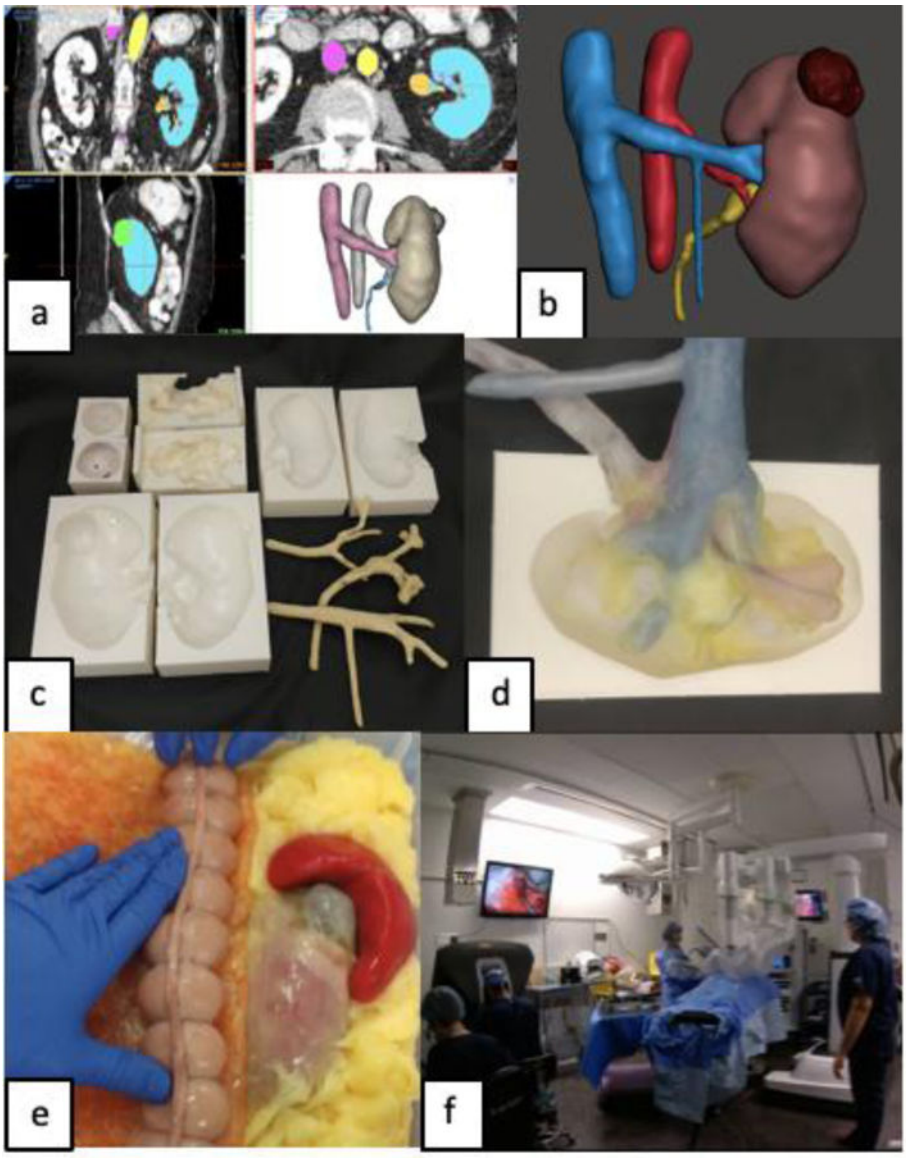

Figure 1:

a) Segmentation of patient CT scan, b) CAD of patient's renal anatomy, c) 3D printed injection molds (Top row: tumor, hilum, medulla, Bottom row: cortex and positive molds of vessels and calyx), d) Internal registration of hollow hilar structures inside a kidney mold, e) Final partial nephrectomy trainer additionally surrounded with peritoneum, abdominal fat, spleen, bowl, and mesentery, f) Full procedural rehearsal is completed with daVinci robot.

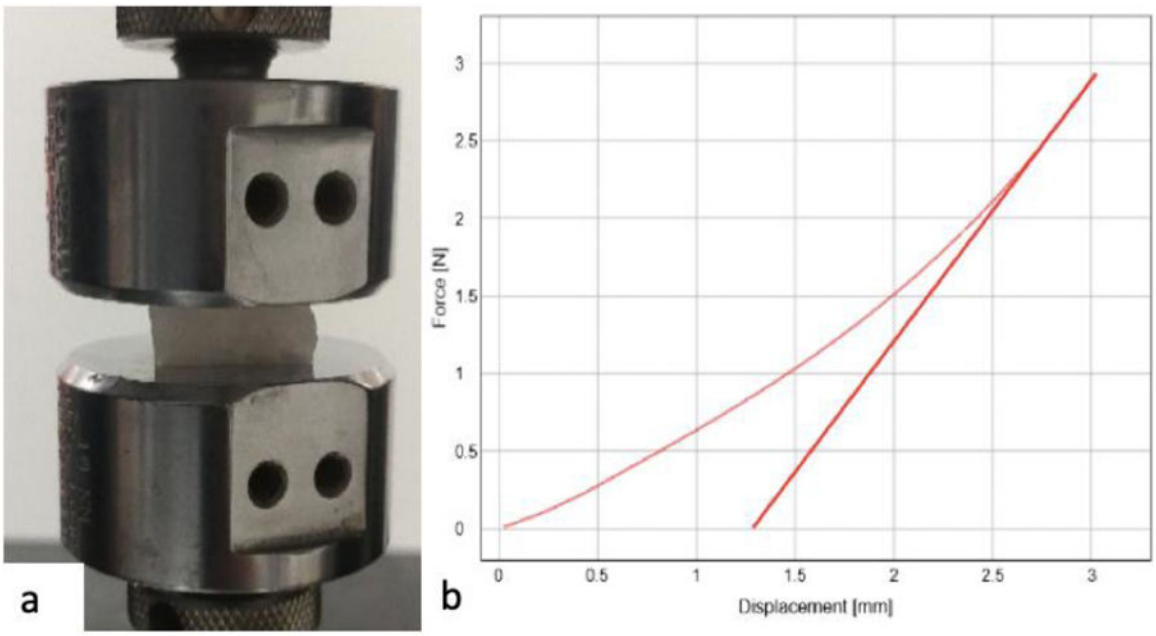

Figure 2:
a) Compression test set up, b) Direct results visible on Bluehill Universal display (curved line) and calculated modulus (straight line).

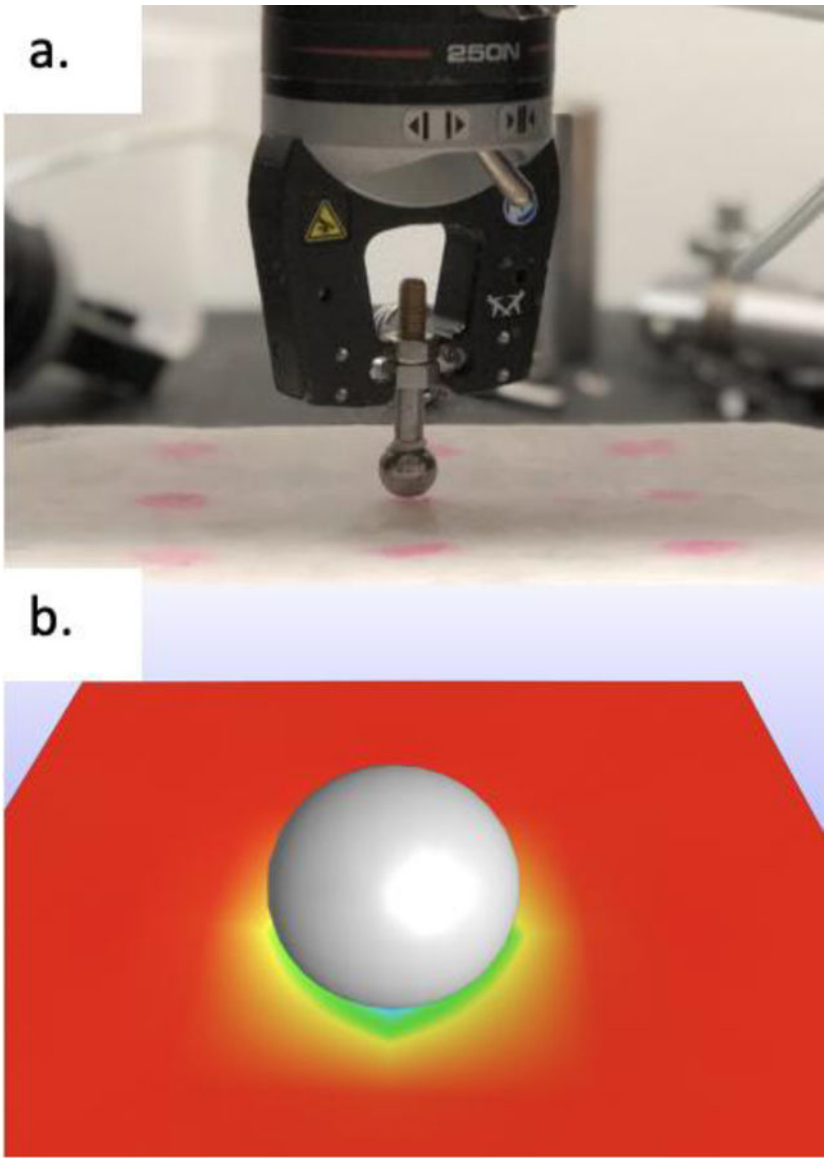

Figure 3:
a) Indentation test set up for 10 PVA, b) IFEA model using FEBio software.

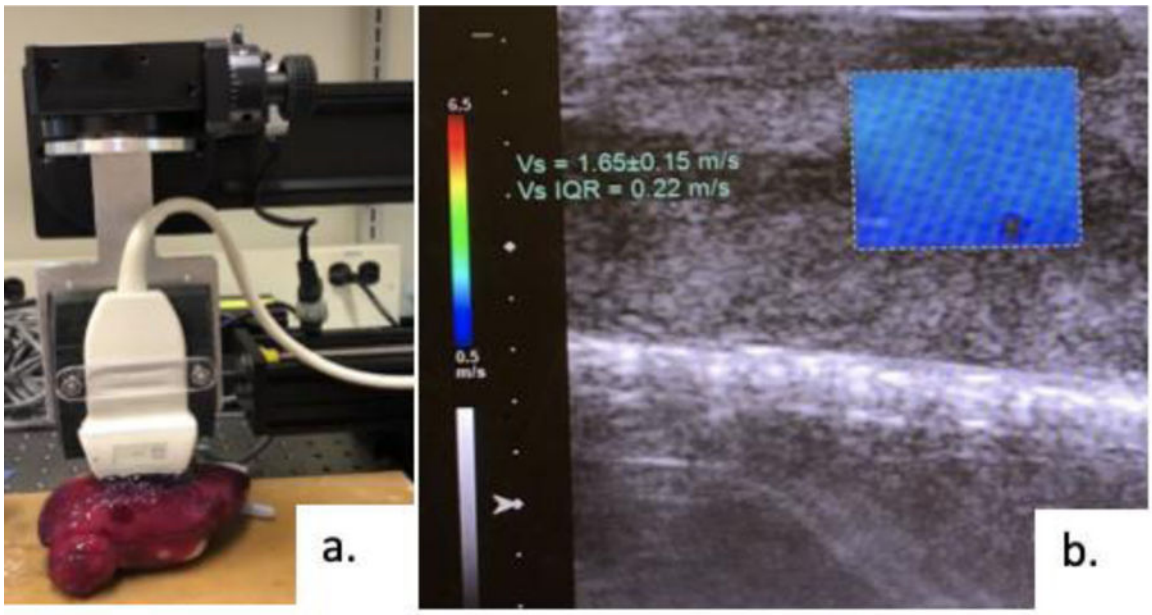

Figure 4:

a) Testing set up with ultrasound probe on PVA kidney, b) Image of ultrasound with area chosen and shear wave speed (V_s) calculated.

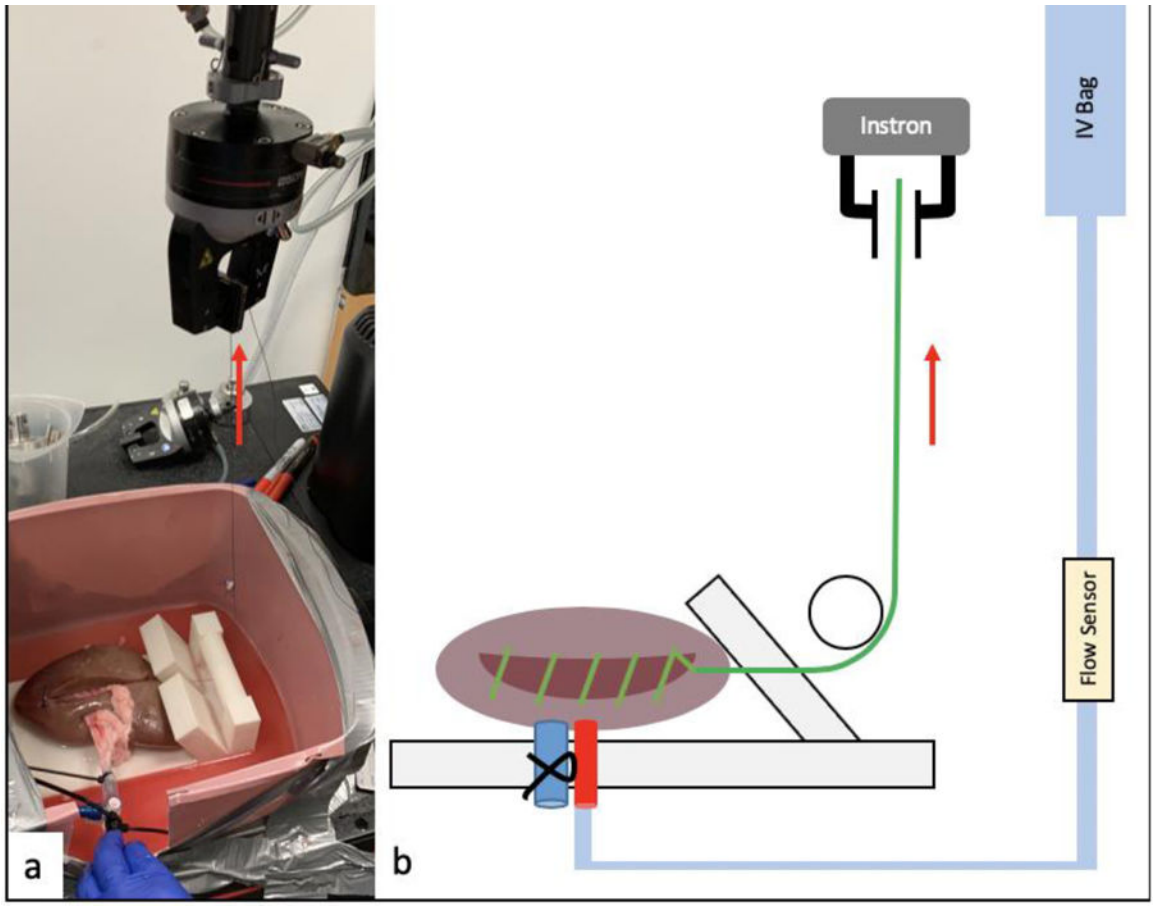

Figure 5:

Perfusion testing set up. Simulated blood is flowing though the catheter secured in the artery, suture is secured to Instron testing instrument to apply the 5 & 10N force to the suture (red arrow). a) Actual setup, b) Graphic illustration of the entire set up.

Figure 6:

Renorrhaphy rip testing set up. a) 3D printed support tray with vertical slits to allow passage of the sutures, b) Visual coaptation of the renal capsule during testing of porcine kidney, c) Clips ripping through the edge of the renal capsule.

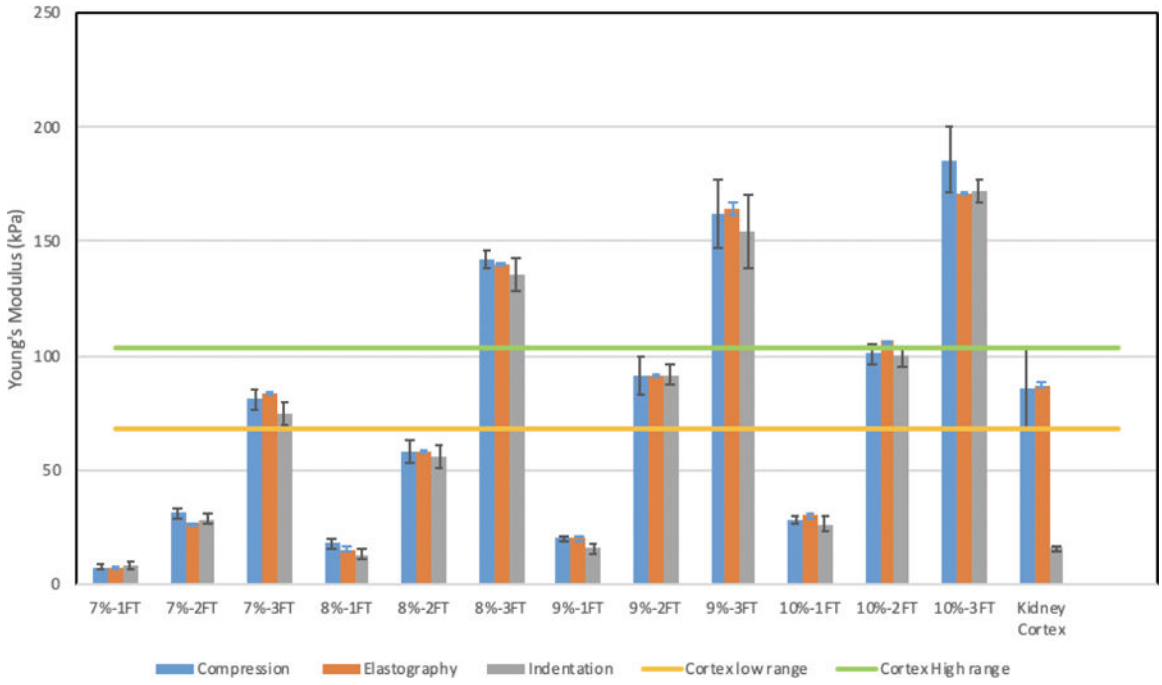

Figure 7:

Kidney mechanical testing. Results for unconfined compression testing (blue), elastography (orange), and indentation testing (grey). The low range (yellow bar) and high range (green bar) represent a ±0.5 SD from mean values of porcine compression testing .7% PVA at 3 freeze-thaw cycles, 9% PVA at 2 freeze-thaw cycles, and 10% PVA at 2 freeze-thaw cycles were chosen as the PVA conditions best suited to replicate porcine kidney tissue properties.

Table 1:

Young's modulus and shear wave speed calculated via a series of mechanical tests

Kidney Cortex samples	**Spherical Indentation testing Mean Young's Modulus (SD), kPa**	**Unconfined compression testing Mean Young's Modulus (SD), kPa**	**Elastography Mean Young's Modulus (SD), kPa**	**Shear wave speed Mean (SD), m/s**
Porcine	**15.7 (± 1.6)**	**85.97 (± 35)**	**87.46 (± 2.97)**	**5.53 (± 1.02)**
7% PVA at 3FT cycles	**74.56 (± 10)**	**80.97 (± 9.05)**	**83.4 (± 0.7)**	**5.4 ± 0.49**
9% PVA at 2FT cycles	**91.91 (± 9.62)**	**91.2 (± 16.9)**	**91.6 (± 0.7)**	**5.66 (± 0.5)**
10% PVA at 2FT cycles	**99.67 (± 9.88)**	**101.1 (± 9)**	**106.4 (± 0.4)**	**6.12 (± 0.36)**

Table 2:

Results of functional testing comparing fresh porcine kidneys to 3 PVA kidney formulations during hemostatic closure tests.

Kidney specimen	Initial flow rate in ml/min	Flow rate in ml/min (% drop) after applying 5N of force	Flow rate in ml/min (% drop) after applying 10N of force
Porcine	120.9	54.5 (55.0%)	41.2 ml/min (65.9%)
7% PVA at 3FT cycles	270.2	115 (57.4%)	80.8 ml/min (70.1%)
9% PVA at 2FT cycles	243.7	187.9 (22.9%)	119.8 ml/min (50.8%)
10% PVA at 2FT cycles	338.7	251.4 (25.8%)	160.9 ml/min (52.5%)

Table 3:

Results of functional testing comparing fresh porcine kidneys to 7% PVA kidney at 3 freeze-thaw cycles during parenchymal capsule approximation and rip tests after applying tension on renorrhaphy Sutures.

Kidney specimen	Average suture tension to approximate renal parenchymal edges Mean (SD)	Average maximum suture tension at which the sutures tear through the renal parenchyma Mean (SD)
Porcine	8.41N (1.38N)	19.29N (8.78N)
7% PVA at 3FT cycles	9.29N (3.07N)	22.36 N (9.8N)